Effect of structural defects on the thermal conductivity of graphene: From point to line defects to haeckelites

Zacharias G. Fthenakis, Zhen Zhu, and David Tománek*
Physics and Astronomy Department, Michigan State University, East Lansing, Michigan 48824, USA
(Received 11 December 2013; revised manuscript received 21 February 2014; published 17 March 2014)

We use nonequilibrium molecular-dynamics simulations to study the effect of structural defects on the thermal conductivity λ of graphene. Focusing on 5-7 and 5-8 defects in the graphene honeycomb lattice, we find that λ depends sensitively on whether the defects are isolated, form lines, or form extended arrangements in haeckelites. Our results indicate that the presence of defects makes λ anisotropic and, depending on the temperature, quenches its value by one to two orders of magnitude with respect to graphene, mainly by reducing the phonon mean free path.

DOI: 10.1103/PhysRevB.89.125421 PACS number(s): 66.70.−f, 63.22.−m, 65.80.−g, 81.05.ue

I. INTRODUCTION

The recent high level of interest in graphene is due primarily to its desirable electronic properties [1]. Much less attention has been paid to another unique property of graphene, namely its high thermal conductivity [2–4]. It turns out that high thermal conductivity is very desirable from the point of view of thermal management, one of the most challenging problems of nanoelectronics [5]. The outstanding thermal conductivity value of $\lambda \approx 5000$ W/m K has been reported in mechanically exfoliated graphene with few defects [4,6], in agreement with theoretical predictions [2]. Graphene grown by chemical vapor deposition (CVD), the only production technique considered viable for large-scale applications, is much more defective. As expected in a growth mechanism with multiple nucleation centers on a substrate, CVD graphene consists of perfect honeycomb lattice regions interconnected by grain boundaries containing lines of nonhexagonal rings of threefold-coordinated carbon atoms. Observed grain boundary structures in CVD graphene include lines of 5-7 defects on Cu [7] and 5-8 defects on Ni(111) [8]. There is strong evidence that thermal transport in graphene is adversely affected by isotopic and structural impurities, including monovacancies, Stone-Thrower-Wales defects, and line defects [6,9–13]. However, there are no reported studies of thermal transport in haeckelite, which we consider a suitable model of structurally disordered CVD graphene. Also, the relative effect of different types of impurities and their spatial arrangement on the net thermal conductivity has not been studied so far.

Here we present computational results for the effect of 5-7 and 5-8 defects, which are common in CVD graphene, on the thermal conductivity λ. Our nonequilibrium molecular-dynamics simulations show that λ depends sensitively on whether the defects are isolated, form lines, or form extended arrangements in haeckelites. Our results indicate that the presence of defects makes λ anisotropic and, depending on the temperature, quenches its value by one to two orders of magnitude with respect to graphene, mainly by reducing the phonon mean free path.

The structural defects we consider in the honeycomb lattice of graphene are nonhexagonal rings arranged in such a way that all carbon atoms are threefold-coordinated [14–16]. Such defects may occur as point defects [17–19], line defects [8,17,20–24], and extended defects [24], which turn graphene into a haeckelite monolayer [16,25–28]. Both periodic [16,24–27,29] and amorphous [30] defect arrangements have been discussed in the literature, with emphasis on structural stability and electronic structure [23,24,27]. Point defects [19,30,31] and line defects [8] have been observed after electron irradiation of graphene. Even though haeckelites have not been synthesized yet, they are believed to have a similar stability to that of C_{60} fullerenes [25–27].

II. COMPUTATIONAL APPROACH

Unlike metals, where electrons contribute significantly to heat conduction, all-carbon structures such as diamond, graphene, and nanotubes owe their high thermal conductivity primarily to phonons. In layered graphitic systems, which we study in the following, the phonon thermal conductivity λ can be expressed as

$$\lambda = (1/2) c_V v_s \langle l \rangle, \tag{1}$$

where c_V is the specific heat per volume, v_s is the speed of sound, and $\langle l \rangle$ is the phonon mean free path. The rigidity of sp^3 and sp^2 carbon bonds is responsible for the high elastic modulus and thus the high speed of sound v_s in diamond and in graphitic structures. Above the Debye temperature, the specific heat is given by the classical Dulong-Petit value and c_V should not change in systems with the same atomic density. The presence of defects in a structure may soften the hard vibrational modes that are a consequence of the rigid bonds, thus lowering the Debye temperature and slightly increasing c_V. The phonon mean free path $\langle l \rangle$ depends on the perfection of the lattice and may achieve large values of the order of a micrometer [4]. Thus, the thermal conductivity of all-carbon structures may be very high, specifically much higher than even the best metal-based heat conductors. Consequently, our study of the thermal conductivity in carbon nanostructures, in particular the role of defects in λ, is based on thermal conduction by phonons. At low defect concentrations, we do not expect significant changes to the specific heat or the speed of sound. Most significant changes to λ will be caused by the reduction of the phonon mean free path.

*tomanek@pa.msu.edu

 ©2014 American Physical Society

Viable approaches to calculate thermal transport in graphitic systems include the phonon Boltzmann equation [32] and molecular-dynamics (MD) simulations. The latter approach, which provides an atomistic description, is unusually demanding computationally in carbon nanostructures with high thermal conductivity. Direct heat flow study using Fourier's law requires establishing a temperature gradient across an interval exceeding the phonon mean free path, which is hard to achieve [2] due to $\langle l \rangle \approx 1\ \mu$m. Similarly, we found that calculations of λ based on the velocity-velocity autocorrelation function using the Green-Kubo formula [33] converge very slowly [2]. Therefore, we make use of the nonequilibrium molecular-dynamics (NEMD) method of Hansen and Evans [34,35], which has been successfully used to study the thermal conductivity of defective carbon nanostructures including graphene and nanotubes [2,9]. While mathematically equivalent to the Green-Kubo formula [34,36], the NEMD approach is computationally much less demanding.

Unlike the previous two MD techniques, the NEMD method introduces a small driving force, characterized by the parameter F_e, which induces a heat flux J_z along a specific direction, taken as z [34,35]. The thermal conductivity λ can then be determined from

$$\lambda = \lim_{F_e \to 0} \lim_{t \to \infty} \frac{\langle J_z(F_e,t) \rangle_t}{F_e T V}, \qquad (2)$$

where V is the volume of the unit cell and T is the temperature. In our calculations, the temperature is controlled by a Nosé-Hoover thermostat [37,38] and the interatomic interactions are described by the Tersoff potential [39]. Unlike in our study of isotopic impurities [9], we considered only isotopically pure carbon systems based on ^{12}C. Our simulations of extended systems have been performed using periodic boundary conditions in order to eliminate finite-size effects. We have used the fifth-order predictor-corrector algorithm of Gear [40] to integrate the equations of motion, with a time step of $\Delta t = 0.2$ fs and $Q = 10$ amu as the thermal inertia of the Nose-Hoover thermostat [9]. Depending on the specific values of F_e and T, we used $N = (2 \times 10^6)$–(5×10^6) as the number of time steps for each simulation.

Prior to each calculation of λ, we have optimized the unit cell and the atomic positions. For each simulation with a specific value of F_e, we determined the value of $\lambda(F_e,T)$ from the time average $\langle J_z(F_e,t) \rangle_t$ of the heat flux J_z according to Eq. (2). The value of $\lambda(T)$ has then been obtained by extrapolating the $\lambda(F_e,T)$ values for $F_e \to 0$. For each specific structure and temperature T, we performed simulations using typically 20 different small values of F_e in order to obtain a reliable extrapolation.

III. RESULTS AND DISCUSSION

A. Point defects

To study the effect of isolated point defects on the temperature-dependent thermal conductivity of graphene, we considered 22.8-Å-long (zigzag direction) and 21.4-Å-wide (armchair direction) unit cells with 180 C atoms and one Stone-Thrower-Wales [41,42] (or 5775) defect, presented in Fig. 1(a). The arrows in the figure indicate the zigzag and the armchair directions along which λ has been calculated.

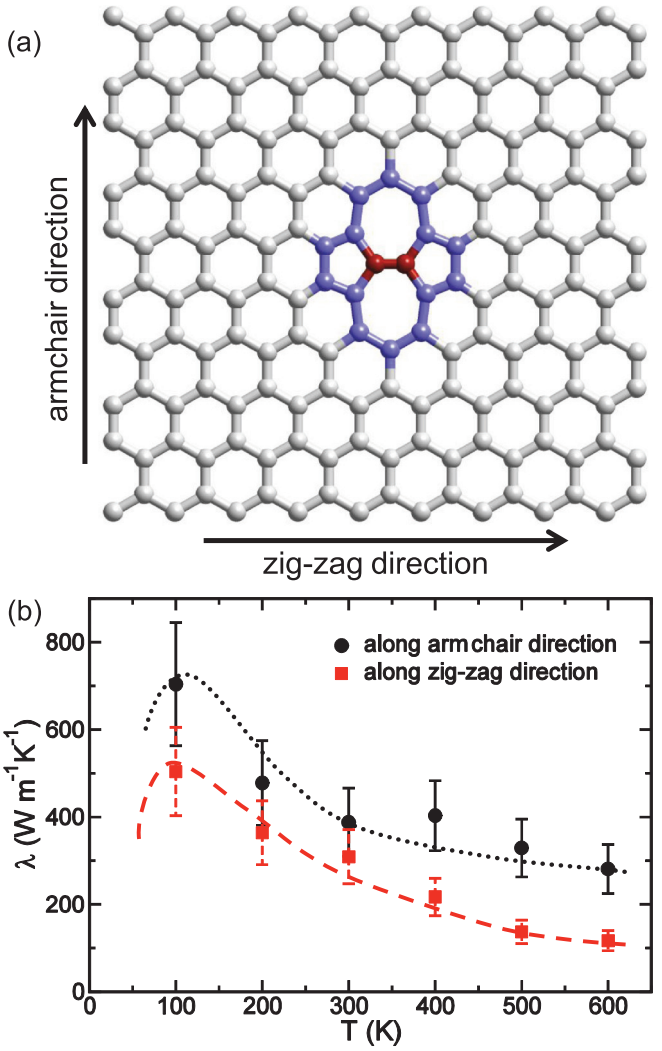

FIG. 1. (Color online) Thermal conductivity of a graphene monolayer with a single 5775 defect, created by a 90° rotation of one bond highlighted in dark red. (a) The 180-atom unit cell used in our simulation. Atoms in the defect region are emphasized by a darker (blue) color. (b) Thermal conductivity λ as a function of temperature T for thermal transport along the zigzag and armchair directions, shown in (a). Lines connecting the data points are guides to the eye.

The general behavior of $\lambda(T)$ can be explained by the temperature dependence of the specific heat c_V and the phonon mean free path $\langle l \rangle$ in Eq. (1). The decrease of λ at high temperatures is caused by the decrease of $\langle l \rangle$. In nature, thermal conductivity decreases at very low temperatures and eventually vanishes at $T = 0$ due to the corresponding trend in c_V. The competition between $\langle l \rangle(T)$ and $c_V(T)$ causes a maximum in $\lambda(T)$, which has been observed [3] at $T \approx 100$ K. Since our classical MD simulations do not reproduce correctly the low-temperature behavior of c_V, the projected maximum in the lines that guide the eye in Fig. 1 represents only an extrapolation of the expected behavior.

Thermal conductivity calculations of defect-free graphene, performed using the same method [2,9], indicate very large values of λ, specifically $\lambda_{\max} \approx 50\,000$ W m^{-1} K^{-1} near 100 K.

Quantitative comparison with these results suggests that even isolated 5775 defects may quench the thermal conductivity by one to two orders of magnitude, depending on temperature T. Still, this type of defective graphene is a better conductor of heat than metallic thermal conductors with typical thermal conductivities of a few hundred W/m K at room temperature.

We found it instructive to compare thermal conductivities in the presence of isolated 5775 defects to our previous results for isolated divacancies [9]. Since the calculated thermal conductivities in the two cases with the same defect concentration [43] were close to each other, we conclude that the precise nature of the structural defect—whether a 5775 defect or a divacancy—plays only a minor role when determining the phonon scattering, which reduces the value of λ.

In view of the near-isotropic thermal conductivity of graphene, the observed anisotropy in Fig. 1(b) is unexpected. In the presence of isolated 5775 defects, we observe a significantly higher value of λ along the armchair direction than along the orthogonal zigzag direction, most likely due to the symmetry breaking at the 5775 defect.

B. Line defects

As mentioned in the Introduction, lines of 5-7 and 5-8 defects commonly occur in graphene grown by CVD on metal substrates [7,8] as a way to accommodate the lattice mismatch. Our present interest lies in the effect of these defect lines and their average separation on the thermal conductivity. We determined λ of graphene modified by a periodic array of defect lines, as shown in Figs. 2(a)–2(c), and we determined the thermal conductivity both parallel and perpendicular to the defect lines. The unit cell width corresponding to the defect line separation L was changed in discrete steps by adding narrow graphene strips, as shown schematically in Fig. 2(a). The length of the unit cell in the direction of the defect lines was kept constant at $d = 20.2$ Å.

We considered lines of 5-7 and 5-8 defects, depicted in Fig. 2(b). As implied by their name, these defects contain pentagonal, heptagonal, and octagonal rings of atoms. Both types of line defects have been observed experimentally [8,20,27] and may be formed by reconstruction at the interface of two adjacent zigzag edges of graphene. In the system with

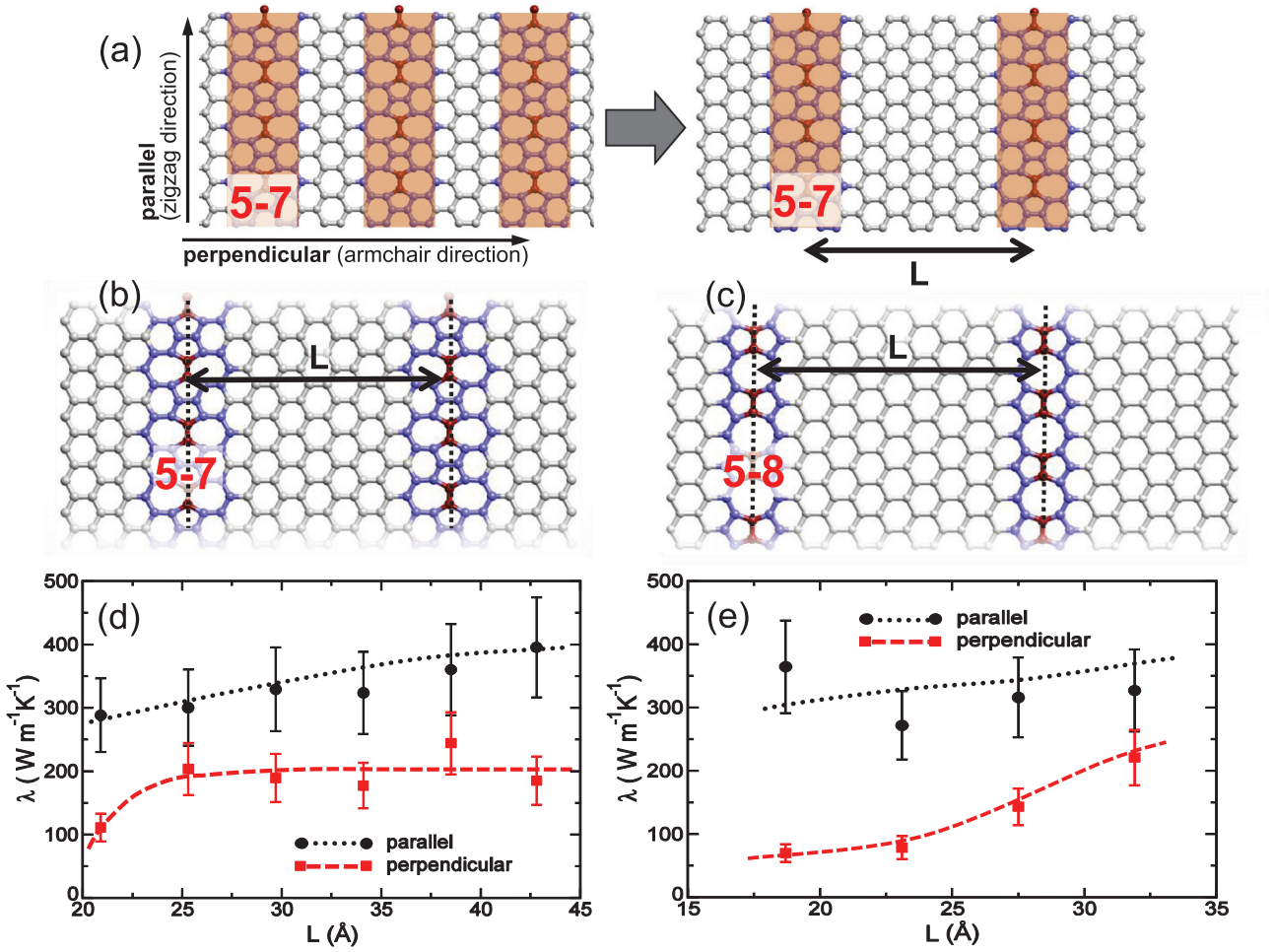

FIG. 2. (Color online) Effect of line defects on the thermal conductivity of a graphene monolayer. (a) Arrangement of 5-7 defect lines, highlighted by shading, which separate graphene strips of different width L, as well as the definition of thermal transport directions. Equilibrium structure of (b) 5-7 and (c) 5-8 defect lines, separated by the distance L. Atoms in nonhexagonal rings are emphasized by the darker color. Bonds rotated by 90° are enhanced by dark red. Thermal conductivity λ of the system with (d) 5-7 and (e) 5-8 line defects as a function of their separation L at $T = 300$ K. Data points for transport parallel and perpendicular to the line defects are connected by dashed and dotted lines as guides to the eye.

5-7 defects, we considered the minimum line separation $L = 20.9$ Å, corresponding to a 160-atom unit cell, and the maximum separation $L = 42.8$ Å, corresponding to a 320-atom unit cell. In the system with 5-8 line defects, we considered the minimum line separation $L = 18.7$ Å, corresponding to a 136-atom unit cell, and the maximum separation $L = 31.9$ Å, corresponding to a 232-atom unit cell.

Our room-temperature thermal conductivity results for an array of 5-7 line defects are presented in Fig. 2(d) and those for 5-8 line defects are presented in Fig. 2(e). We find that both systems display very similar behavior in terms of thermal conductivity. We observe a clear anisotropy indicating better heat conduction in the direction of line defects than perpendicular to the defect lines. Whereas λ in the direction of line defects increases gradually with increasing L from 250 to 400 W/m K, its values are still about one order of magnitude below the room-temperature value $\lambda = 5000$ W/m K in defect-free graphene [2,9].

Bearing in mind that λ should reach the value of a defect-free graphene monolayer for L exceeding the phonon mean free path of graphene $\langle l_g \rangle$, we conclude that the relatively low thermal conductivity values are caused by a strong reduction of the phonon mean free path in the graphene nanoribbons by scattering at the defect lines. The same trend for λ has been reported for graphene nanoribbons with line defects [44] and is in line with our previous study of finite-width graphene nanoribbons, where free edges play the same role as defect lines in the present case [9]. As a crude way to estimate the thermal conductivity of defect-free graphene by extrapolating our results, we estimate the slope of λ parallel to the defect lines to be $\Delta\lambda/\Delta L \lesssim 4$ W/(m K Å). Assuming this slope to remain constant up to the experimentally observed value [4] $\langle l_g \rangle \approx 775$ nm, we find $\lambda(L = \langle l_g \rangle) \lesssim 30\,000$ W/m K, in rough agreement with the observed value.

We find the thermal conductivity perpendicular to the defect lines to be significantly smaller, ranging between $\lambda = 50$ and 250 W/m K. Whereas the values are rather independent of L in the 5-7 system, λ seems to increase with increasing L in the 5-8 system. We should not depend on these results for a limited range of L values to predict a trend, but we must consider the fact that thermal conduction normal to the defect lines will be limited by phonon transmission across these lines. In any case, we find the value range of λ at room temperature, presented in Figs. 2(d) and 2(e), to be similar to the calculated thermal conductivity in the presence of isolated 5775 defects, shown in Fig. 1(b). We conclude that isolated defects scatter as efficiently as line defects of the same type.

C. Haeckelites

To complete our study of thermal conductivity in defective graphene, we considered the entire graphene monolayer

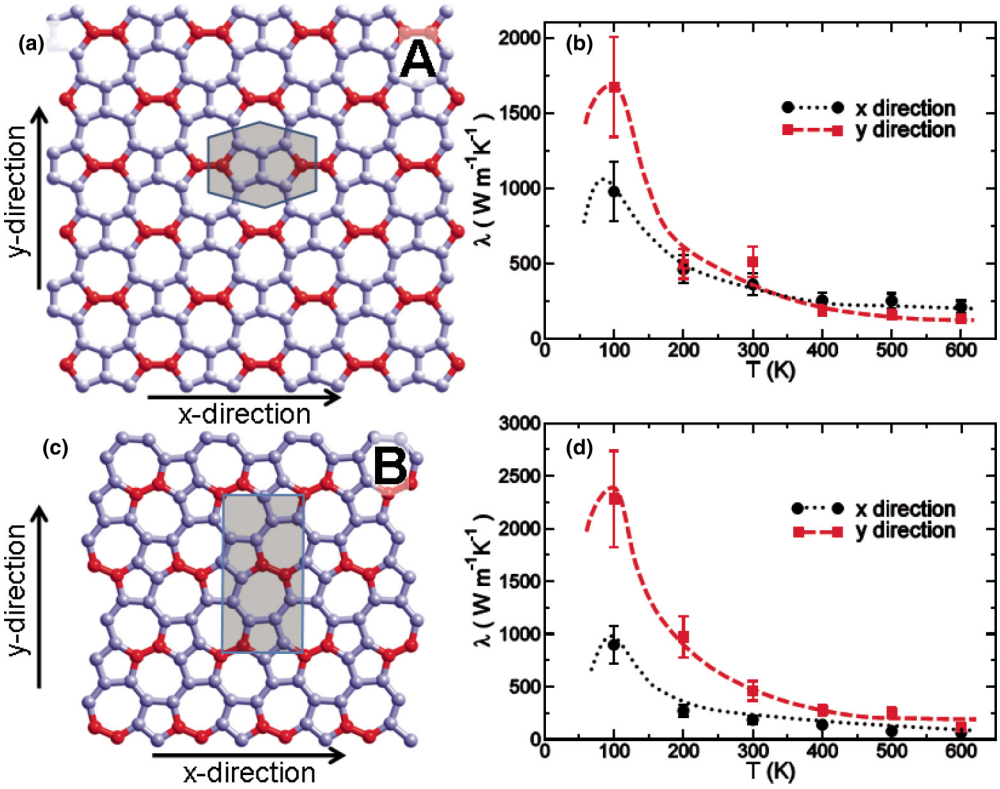

FIG. 3. (Color online) Different structural arrangements of 5-7 rings in two prototypical haeckelite structures and their effect on the thermal conductivity. (a) The 192-atom unit cell of haeckelite A used in the calculation and the eight-atom primitive unit cell enhanced by shading. (b) Temperature dependence of the thermal conductivity of haeckelite A along the two directions shown in (a). (c) The 128-atom unit cell of haeckelite B used in the calculation and the 16-atom primitive unit cell enhanced by shading. (d) Temperature dependence of the thermal conductivity of haeckelite B along the two directions shown in (b). The haeckelite structures in (a) and (c) have been obtained from the graphene structure by rotating the bonds highlighted by the dark red color. Lines connecting the data points in (b) and (d) are guides to the eye.

transformed by bond rotations to a planar periodic arrangement of pentagons and heptagons, called haeckelite. We consider two such pentaheptites as the simplest haeckelite structures. The atomic arrangement in pentaheptite "A" is shown in Fig. 3(a) and that of pentaheptite "B" is shown in Fig. 3(c). The primitive unit cell of pentaheptite A, highlighted by the shaded region in Fig. 3(a), contains eight atoms. Our calculations for pentaheptite A were performed using a 4×6 superlattice with 23.2-Å-long (x direction) and 22.44-Å-wide (y direction) supercells containing 192 atoms, as seen in Fig. 3(a).

The primitive unit cell of pentaheptite B, highlighted by the shaded region in Fig. 3(c), contains 16 atoms. Our calculations for pentaheptite B were performed using 19.33-Å-long (x direction) and 18.51-Å-wide (y direction) 2×4 supercells containing 128 atoms, shown in Fig. 3(c).

We determined the thermal conductivity along the orthogonal x and y directions, which corresponded to the zigzag and armchair directions in the initial graphene layer prior to its conversion to a pentaheptite by a series of Stone-Wales transformations [41]. Our numerical results for the thermal conductivity of pentaheptite A are presented in Fig. 3(b) and those for pentaheptite B are presented in Fig. 3(d) in the temperature range between 100 and 600 K. Even though both haeckelite structures are periodic and contain only threefold-coordinated atoms, their thermal conductivities are comparable to that of graphene with isolated 5775 defects in Fig. 1(b), namely more than one order of magnitude lower than a graphene monolayer. Similar to our results for isolated 5775 defects, we find the thermal conductivity of both pentaheptites to be anisotropic due to the symmetry breaking of the lattice. The qualitative behavior of λ is the same in pentaheptite A and B. Unlike in pentaheptite B, the direction of the most efficient heat transfer in pentaheptite A changes from the y direction for $T \lesssim 300$ K to the x direction at higher temperatures according to Fig. 3(b).

To understand why the thermal conductivity of haeckelites should be more than one order of magnitude lower than that of graphene, we inspected Eq. (1) for possible causes. Since our classical molecular-dynamics simulations reproduce the Dulong-Petit value of c_V that is independent of temperature and system, the observed reduction of λ in haeckelites is unrelated to the specific heat. Another possible cause for this behavior could be a change in the speed of sound v_s. We have determined v_s from the slope $d\omega(\mathbf{k})/dk$ of the acoustic branches in the vibration spectrum near the Γ point. Unlike in graphene, we found the phonon-dispersion relations of the pentaheptites A and B to be somewhat anisotropic around Γ. The maximum values of the speed of sound were found to be $v_s(A) = 19\,700$ m/s in pentaheptite A and $v_s(B) = 20\,000$ m/s in pentaheptite B, both about 18% lower than the graphene value $v_s(g) = 24\,000$ m/s. Thus, this reduction in v_s alone cannot explain the reduction in the thermal conductivity of over one order of magnitude when comparing haeckelite to graphene. Consequently, it is the reduction of the phonon mean free path that plays the critical role when comparing haeckelite to graphene. Based on the observed value [4] of the phonon mean free path $\langle l_g \rangle \approx 775$ nm in graphene at $T = 300$ K, we estimate the phonon mean free path of haeckelites to be of the order of 90 nm at room temperature.

IV. CONCLUSIONS

We have performed nonequilibrium molecular-dynamics simulations to study the effect of structural defects on the thermal conductivity λ of graphene. We considered structural defects that preserve the threefold coordination of all carbon atoms and that include pentagonal, heptagonal, and octagonal carbon atom rings. Focusing on 5-7 and 5-8 defects in the graphene honeycomb lattice, we find that λ depends sensitively on whether the defects are isolated, form lines, or form extended arrangements in haeckelites. We found that the presence of nonhexagonal rings in the graphene lattice makes λ anisotropic, which can be understood by symmetry breaking. Depending on the temperature, the high thermal conductivity of graphene is quenched by one to two orders of magnitude in the presence of such defects, mainly by reducing the phonon mean free path. We find the reduction of λ due to the presence of nonhexagonal rings in the graphene lattice to be comparable in magnitude to that caused by divacancies at the same concentration. In systems containing arrays of parallel line defects, we find the quenching of λ in the direction of defect lines to be comparable to that of narrow graphene nanoribbons. These results indicate that the main reason for the reduction of the thermal conductivity in defective systems is a decrease in the phonon mean free path. We found that phonons are scattered similarly by nonhexagonal ring defects and by natural boundaries such as edges and vacancies. In the haeckelite systems considered here, which consist of a periodic arrangement of 5-7 rings, we find that the phonon mean free path is strongly reduced with respect to graphene, and we estimate its value to be $\approx$90 nm at room temperature.

ACKNOWLEDGMENTS

This work was funded by the National Science Foundation Cooperative Agreement No. EEC-0832785, titled "NSEC: Center for High-rate Nanomanufacturing." Computational resources have been provided by the Michigan State University High Performance Computing Center.

[1] A. H. Castro Neto, F. Guinea, N. M. R. Peres, K. S. Novoselov, and A. K. Geim, Rev. Mod. Phys. **81**, 109 (2009).

[2] S. Berber, Y.-K. Kwon, and D. Tomanek, Phys. Rev. Lett. **84**, 4613 (2000).

[3] A. A. Balandin, S. Ghosh, W. Bao, I. Calizo, D. Teweldebrhan, F. Miao, and C. N. Lau, Nano Lett. **8**, 902 (2008).

[4] S. Ghosh, I. Calizo, D. Teweldebrhan, E. P. Pokatilov, D. L. Nika, A. A. Balandin, W. Bao, F. Miao, and C. N. Lau, Appl. Phys. Lett. **92**, 151911 (2008).

[5] E. Pop, S. Sinha, and K. E. Goodson, Proc. IEEE **94**, 1587 (2006).

[6] S. Chen, Q. Wu, C. Mishra, J. Kang, H. Zhang, K. Cho, W. Cai, A. A. Balandin, and R. S. Ruoff, Nat. Mater. **11**, 203 (2012).
[7] P. Y. Huang, C. S. Ruiz-Vargas, A. M. van der Zande, W. S. Whitney, M. P. Levendorf, J. W. Kevek, S. Garg, J. S. Alden, C. J. Hustedt, Y. Zhu, J. Park, P. L. McEuen, and D. A. Muller, Nature (London) **469**, 389 (2011).
[8] J. Lahiri, Y. Lin, P. Bozkurt, I. I. Oleynik, and M. Batzill, Nat. Nanotechnol. **5**, 326 (2010).
[9] Z. G. Fthenakis and D. Tománek, Phys. Rev. B **86**, 125418 (2012).
[10] F. Hao, D. Fang, and Z. Xu, Appl. Phys. Lett. **99**, 041901 (2011).
[11] A. Bagri, S.-P. Kim, R. S. Ruoff, and V. B. Shenoy, Nano Lett. **11**, 3917 (2011).
[12] Y. Lu and J. Guo, Appl. Phys. Lett. **101**, 043112 (2012).
[13] A. Y. Serov, Z.-Y. Ong, and E. Pop, Appl. Phys. Lett. **102**, 033104 (2013).
[14] M. Deza, P. W. Fowler, M. Shtogrin, and K. Vietze, J. Chem. Inf. Comput. Sci. **40**, 1325 (2000).
[15] H. Zhu, A. T. Balaban, D. J. Klein, and T. P. Zivkovic, J. Chem. Phys. **101**, 5281 (1994).
[16] M. T. Lusk and L. Carr, Carbon **47**, 2226 (2009).
[17] H. Terrones, R. Lv, M. Terrones, and M. S. Dresselhaus, Rep. Progr. Phys. **75**, 062501 (2012).
[18] B. W. Jeong, J. Ihm, and G.-D. Lee, Phys. Rev. B **78**, 165403 (2008).
[19] A. Hashimoto, K. Suenaga, A. Gloter, K. Urita, and S. Iijima, Nature (London) **430**, 870 (2004).
[20] T. Hu, J. Zhou, J. Dong, and Y. Kawazoe, Phys. Rev. B **86**, 125420 (2012).
[21] M. T. Lusk and L. D. Carr, Phys. Rev. Lett. **100**, 175503 (2008).
[22] M. T. Lusk, D. T. Wu, and L. D. Carr, Phys. Rev. B **81**, 155444 (2010).
[23] D. J. Appelhans, Z. Lin, and M. T. Lusk, Phys. Rev. B **82**, 073410 (2010).
[24] D. J. Appelhans, L. D. Carr, and M. T. Lusk, New J. Phys. **12**, 125006 (2010).
[25] V. H. Crespi, L. X. Benedict, M. L. Cohen, and S. G. Louie, Phys. Rev. B **53**, R13303 (1996).
[26] H. Terrones, M. Terrones, E. Hernández, N. Grobert, J.-C. Charlier, and P. M. Ajayan, Phys. Rev. Lett. **84**, 1716 (2000).
[27] C. Su, H. Jiang, and J. Feng, Phys. Rev. B **87**, 075453 (2013).
[28] A. N. Enyashin and A. L. Ivanovskii, Phys. Status Solidi B **248**, 1879 (2011).
[29] X.-Q. Wang, H.-D. Li, and J.-T. Wang, Phys. Chem. Chem. Phys. **15**, 2024 (2013).
[30] J. Kotakoski, A. V. Krasheninnikov, U. Kaiser, and J. C. Meyer, Phys. Rev. Lett. **106**, 105505 (2011).
[31] J. C. Meyer, C. Kisielowski, R. Erni, M. D. Rossell, M. F. Crommie, and A. Zettl, Nano Lett. **8**, 3582 (2008).
[32] L. Lindsay, D. A. Broido, and N. Mingo, Phys. Rev. B **80**, 125407 (2009).
[33] D. A. McQuarrie, *Statistical Mechanics* (Harper & Row, London, 1976).
[34] D. J. Evans, Phys. Lett. A **91**, 457 (1982).
[35] D. P. Hansen and D. J. Evans, Mol. Phys. **81**, 767 (1994).
[36] M. J. Gillan and M. Dixon, J. Phys. C **16**, 869 (1983).
[37] S. Nosé, J. Chem. Phys. **81**, 511 (1984).
[38] W. G. Hoover, Phys. Rev. A **31**, 1695 (1985).
[39] J. Tersoff, Phys. Rev. Lett. **61**, 2879 (1988).
[40] C. W. Gear, Argonne National Laboratory Report No. 7126, 1966 (unpublished).
[41] A. Stone and D. Wales, Chem. Phys. Lett. **128**, 501 (1986).
[42] P. A. Thrower, *The Study of Defects in Graphite by Transmission Electron Microscopy*, Chemistry and Physics of Carbon Vol. 5 (Marcel Dekker, New York, 1969), pp. 217–320.
[43] For the sake of consistency, we define the concentration of defects by the fraction of atoms with a locally changed bonding geometry in the entire structure.
[44] J. Haskins, A. Kinaci, C. Sevik, H. Sevinçli, G. Cuniberti, and T. Çağin, ACS Nano **5**, 3779 (2011).